Eur. Phys. J. B (2018) 91: 90
https://doi.org/10.1140/epjb/e2018-90006-0

THE EUROPEAN PHYSICAL JOURNAL B

Regular Article

Collective motion of magnetization in two-dimensional arrays of square elements

Petr D. Kim[1], Vitaly A. Orlov[1,2,a], Roman Yu. Rudenko[1,2], Aleksandr V. Kobyakov[1,2], Anna V. Lukyanenko[1,2], Vladimir S. Prokopenko[3], Irina N. Orlova[3], and Tatyana V. Rudenko[2]

[1] Kirensky Institute of Physics, Krasnoyarsk Scientific Center, Russian Academy of Sciences, Siberian Branch, Krasnoyarsk 660036, Russia
[2] Siberian Federal University, Krasnoyarsk 660041, Russia
[3] Krasnoyarsk State Pedagogical University after V.P. Astaf'ev, Krasnoyarsk 660049, Russia

Received 3 January 2018 / Received in final form 18 March 2018
Published online 30 May 2018 – © EDP Sciences, Società Italiana di Fisica, Springer-Verlag 2018

Abstract. The resonance in a two-dimensional array of square ferromagnetic elements has been experimentally investigated. The magnetization of the elements is shown to be in the vortex state. The resonance peak splitting in the array with increasing density of the elements has been established. The explanation of this phenomenon is proposed and eigenfrequencies of the collective modes are theoretically estimated. Different combinations of polarities and chiralities of the nearest elements in the array are examined.

1 Introduction

Over the years, there has been a keen interest in studying nanosized objects. This is due to the prospects of their application in ultrahigh density data storage, spintronics, and micro- and nanosurgery. Under certain conditions, the magnetization of micro- and nanosized elements demonstrates the vortex distribution [1]. The competition between the exchange and demagnetizing energies leads to the formation of a region with the strongly inhomogeneous magnetization at the vortex core center. The core magnetic moment is perpendicular to the element plane. The characteristic core radius can be estimated as $\delta \approx \sqrt{A/(4\pi M_S)}$, where A is the exchange constant and M_S is the saturation magnetization. The δ value for most magnetically soft materials is about ten nanometers.

The dynamic properties of magnetization are theoretically described by the Landau-Lifshitz-Gilbert (LLG) equation and its modification proposed by Thiele [2]. The method proposed in [2] consists in the following. The equation of magnetization motion in magnets with soliton inhomogeneities is rewritten in the collective variables (coordinate and velocity of the soliton core). Thus, the LLG equation takes the so-called non-Newtonian form [3,4]. The core trajectory consists of helical figures. This was confirmed by the numerical simulation and attempts of direct observation [5–7]. It is worth noting that the magnetization of nanospots with the noncircular (nonelliptical) shape is more complex.

Modern technology makes it possible to synthesize arrays of ferromagnetic micro- and nanoelements of different shapes (circular, square, triangular, etc.). In micron and submicron square magnets, a structure from triangular domains separated by 90-degree Neel walls is implemented. In the close vicinity of the square center, at a spot of domain wall intersection, the vortex structure occurs. When the core is shifted from the square center, demagnetizing fields induce the effective restoring force and gyroforce. The latter is caused by spin precession in the effective field of a magnet. The core motion around the square center is similar to the Larmor precession of a charged particle around the magnetic induction lines. The frequency of this rotation is hundreds of MHz. This is noticeably lower than the frequency of the classical ferromagnetic resonance (FMR) with the moving domain walls involved. Note that in square elements, both regimes of the magnetization motion were observed experimentally [8]. The large difference between the frequencies suggests that the domain structure affects insignificantly the gyrotropic motion of the vortex core.

The state of magnetization in an individual element is characterized by the two parameters: the core polarity $p = \pm 1$, i.e., the core magnetic moment direction (parallel or antiparallel to the separated direction of the Z axis) and the core chirality $q = \pm 1$, i.e., the direction of magnetization in a magnetic core (clockwise or counterclockwise). The methods for controlling (observing) the magnetization state in submicron magnets have been fairly well-developed. They include force microscopy [9–12] The polarity and chirality in the resonance mode are governed by short current pulses (see, e.g., [13,14]) and field pulses [15–18]; in the arrays of square elements, the gradient fields effectively work [19].

The development of high-density data storage devices requires the density of elements in an array to be maximum high. In such arrays, the magnetization dynamics is

[a] e-mail: orlhome@rambler.ru

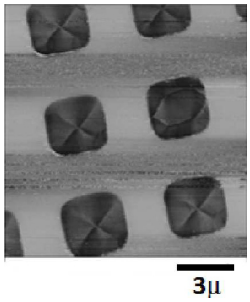

Fig. 1. Force microscopy image of the magnetization structure for a part of the array of square elements.

significantly affected by the interaction of magnetic subsystems. This is, as a rule, the magnetostatic interaction; however, the indirect exchange by conduction electron [20] and direct exchange (in the presence of magnetic bridges between neighboring elements [21]) can also take place. Therefore, in recent years, a great number of experimental and theoretical studies on the effect of interparticle interaction on the static and dynamic magnetic properties of arrays have been published.

Theoretical calculations are often based on the model concepts in which the magnetostatic interaction is specified in the dipole approximation. In particular, in fundamental works [22–26], the dispersion laws for 1D and 2D arrays were analytically calculated with regard to the dipole interaction of core magnetic moments. The authors of [24,27] established the dispersion laws in the model of an array of circular elements with the identical chirality and alternating polarity. For arrays with a great number of microdots and in small sets [28–30], the elimination of degeneracy of the resonant frequency due to the magnetostatic interaction was predicted and observed.

In most of the above-mentioned works, the calculations were performed with disregard of the dissipation and only for few combinations of polarities and chiralities. This study was aimed at filling in this gap for the case of an array of micron square elements.

2 Experimental

An array of square nanodots was formed from a continuous film by the lift-off technique using thermal evaporation of a 80HXC alloy in high vacuum and deposition onto the silicon substrate coated with a photoresist. The desired morphology was formed on the substrate surface using an AZ Nlof 2035 negative photoresist. The magnetic structure of ferromagnetic nanospots was studied on a Veeco MultiMode NanoScope IIIa scanning probe microscope. Figure 1 shows a characteristic scan of the magnetic structure obtained using a two-pass technique in the cantilever frequency modulation regime. The backward pass height was $z_0 = 50\,\text{nm}$. The obtained images allowed us to conclude that the structure most frequently forming in squared elements is equilibrium with the closed magnetic flux and consists of four domains separated by 90-degree walls. At the square center (at the intersection of diagonals), there is a core, as at the center of circular elements.

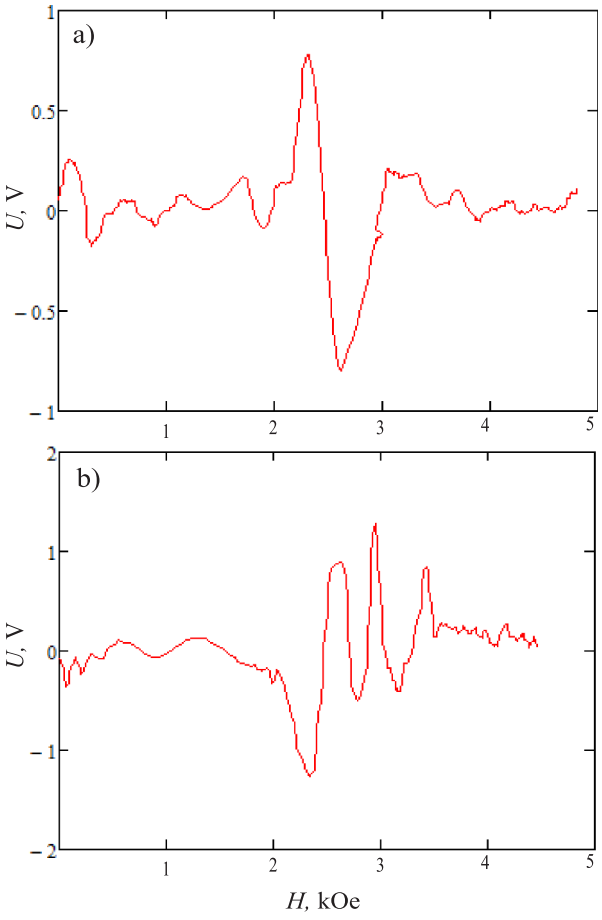

Fig. 2. Differential absorption curves for the array of square elements with distances of (a) 9 and (b) 5 μm between centers.

The square element side length is $a \approx 3\,\mu\text{m}$ and the thickness is $L \approx 12\,\text{nm}$.

The resonance behavior of magnetization was experimentally investigated on a FMR spectrometer. The sample was placed in the antinode of a high-frequency magnetic field ($\omega = 415\,\text{MHz}$). The amplitude of the ac magnetic field applied in the nanodisk plane was 1 Oe. The main field was applied perpendicular to the waveguide plane. The signal from the sample was amplified by a selective amplifier at a modulation frequency of 1 kHz and supplied to a synchronous detector. The main field H varied from 0 to 5 kOe. The obtained differential curves are presented in Figure 2.

It can be seen in Figure 2 that at large distances between elements in the array, the only absorption peak is observed. In this case, the interplay of elements is negligible. The observed peak corresponds to the resonant motion of core vortices in the elements where the combination of polarity and chirality signs is favorable for a specified direction and value of the main field. At small distances between elements, the interaction of the latter leads to the cooperative motion of cores. At certain combinations of the polarity and chirality, different vibrational modes are excited. As a result, we observe a set of resonant

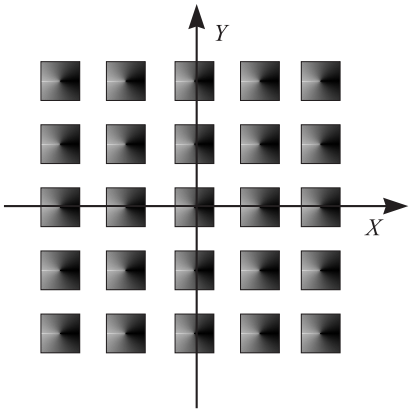

Fig. 3. Model of a two-dimensional array of square elements.

frequencies. Since there is neither direct contact nor magnetic bridges between elements, it would be reasonable to suggest that the elements interact via magnetostatics.

Since we could not control the chirality during sample fabrication, the parameter q of elements in the array was randomly distributed. According to the force microscopy data, the film is divided into the so-called islands formed by families of elements with the identical chirality. The number of magnets in such islands varies in wide ranges. The same polarity p can be ensured by magnetizing a film to saturation in the direction perpendicular to the surface in the resonance mode.

3 Results and discussion

The authors of [25] proposed an exact technique for calculating the energy of interaction between elements. The technique is based on the Fourier transform of demagnetizing factors, which depend on the shape of elements. The approach described in [25] is highly effective, in particular, for solving a problem on the interaction of magnetic moments of the vortex cores. The use of this technique in the case of square elements with the nonuniform magnetization distribution and in-plane magnetic moment component is complicated. Therefore, to make the estimation with regard to the damping, we use the approach proposed in [11,31].

We consider a model that allows us to qualitatively understand the origin of FMR frequency splitting. In the investigated 2D array, the centers of square ferromagnetic elements are separated by the same distance d (Fig. 3).

In ac magnetic fields of relatively low frequencies ($\leq$1 GHz), the core behavior is similar to the gyrotropic motion of a quasiparticle in the field of effective forces [32–37]. The Thiele equation has the form

$$\mathbf{G} \times \mathbf{v} - D\mathbf{v} - \nabla U = 0. \quad (1)$$

Here, γ is the gyromagnetic ratio, $\mathbf{G}$ is the gyrovector, $\mathbf{v}$ is the magnetic vortex core velocity vector, D is the effective viscous friction coefficient, and U is the effective potential energy of the core. The gyrovector can be presented in the form [13,36,38]: $\mathbf{G} = \pi_T G_0(1 - ph)\mathbf{k}$, where $\pi_T = pq$ is the topological charge of the magnetic core [39,40], $G_0 = 2\pi M_S L/\gamma$, $h = H_z/H_S$, $H_S \approx 10$ kOe is the saturation field in the z axis direction, and L is the square thickness. The z axis is perpendicular to the film surface (its unit vector is $\mathbf{k}$). We can write the energy U as

$$U = U_p + U_{\text{dip}} + U_H. \quad (2)$$

Here, U_H is the energy of interaction of the magnetic subsystem of an element with the external magnetic field and U_p is the potential energy of the core, which increases with the core shift from the equilibrium position (spot center) due to the increasing demagnetizing fields. At the small core shift from the equilibrium position, we can write $U_p = \kappa\mathbf{r}^2/2$, where $\kappa = \kappa_0(1 - h^2)$ is the effective stiffness of the quasielastic force acting on the core [13,36,38], and $\mathbf{r}$ is the radius vector of the core center with the beginning at the square center. The question about the explicit dependence of the parameter D on the parameters of magnetic elements is fairly complex. An analytical expression is difficult to obtain. In this work, we used the estimates reported in [41–44].

The quantity U_{dip} describes the energy of pair magnetostatic interaction between elements of the array. We propose to separate the interaction between magnetic moments of the vortex cores, which is relatively weak due to the small volume of the cores [45], and the interaction between magnetic charges on the side faces of the squares. The former is independent of the core coordinate and the latter, which can be strong enough, occurs between the induced magnetic moments due to the core shift from the magnet center and can be effectively estimated by a magnetic charge technique in the rigid vortex model [46,47].

The dependence of the interaction value on the distance between particles in the array was studied in several works. The authors of [48,49] showed that without external field the energy of interaction is proportional to d^{-6}. The interplay of magnetic subsystems of a pair of elements induces the effect analogous to the polarization of gas molecules; therefore, the authors of [48,49] mentioned the analogy with the van der Waals forces. As was shown in [43], in the presence of external magnetic field the energy of pair interaction obeys the dependence $\sim d^{-3.6}$. The depression can be explained taking into account the relative weakness of the magnetostatic interaction as compared with the Zeeman energy at the fields that can significantly change the effective parameters G and κ. As the external field increase, the quality of dipole approximation in describing the energy of interaction is enhanced. The authors of [24] proposed a method for the strict calculation of the dependence of interparticle interaction energy on d. The authors of [24] showed that in the absence of external magnetic field the expression for the magnetostatic interaction energy is presented as a series in terms of uneven degrees $1/d$.

Here, we limit the consideration to the dipole interaction with the energy decreasing in accordance with the law $\sim d^{-3}$. It is applicable at slight shifts of the core from the equilibrium position. We present the terms from equation (2) as functions of the core coordinate. The

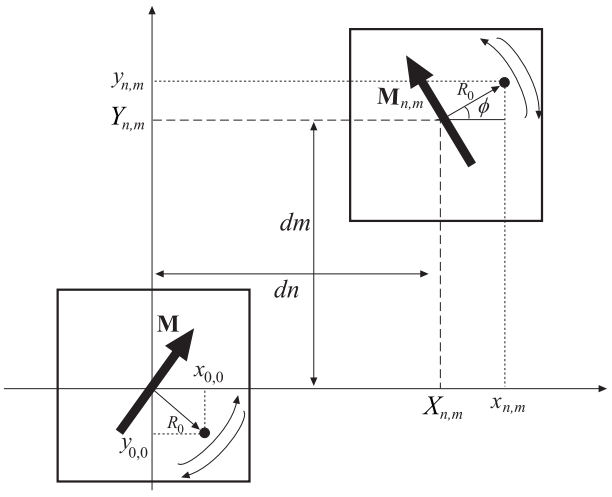

Fig. 4. System of coordinates and schematic of magnetostatic interaction between square elements. The dot shows the vortex core position and the bold arrow, the magnetic moment direction. In both disks, the same chirality $q = 1$ is chosen (the magnetization direction near the core is clockwise). Thin arrows at the disk edge show possible core motion directions.

energy of interaction between two elements distant from each other by n periods in the horizontal direction and m periods in the vertical direction (Fig. 4) is

$$W_{n,m} = \frac{\mu_0}{4\pi(n^2+m^2)^{3/2}d^3} \times \left(\mathbf{M}\mathbf{M}_{n,m} - 3\frac{(\mathbf{M}\mathbf{r}_{n,m})(\mathbf{M}_{n,m}\mathbf{r}_{n,m})}{(n^2+m^2)d^2}\right). \quad (3)$$

Here, $\mathbf{r}_{n,m}$ is the radius vector connecting the centers of the investigated squares. Figure 4 illustrates how the value and orientation of the magnetic moment $\mathbf{M}$ of an element depends on the core coordinates. The projections of the magnetic moment of an element onto the coordinate axes can be written in the form $M_x = -qM\sin(\phi) = -qMy/R_0$, $M_y = qM\cos(\phi) = qMx/R_0$. Then, the energy of interaction of the separated element with the rest matrix is

$$\begin{aligned} U_{\mathrm{dip}} &= \frac{\mu_0}{4\pi}\frac{q_{0,0}M^2}{d^3R_0^2}\sum_{(n+m)\neq 0}\left(q_{n,m}\frac{y_{0,0}y_{n,m}+x_{0,0}x_{n,m}}{(n^2+m^2)^{3/2}}\right. \\ &\quad -\frac{3q_{n,m}}{(n^2+m^2)^{5/2}}(-y_{0,0}n+x_{0,0}m) \\ &\quad \left.\times(-y_{n,m}n+x_{n,m}m)\right) \\ &= \varepsilon\sum_{(n+m)\neq 0}\frac{q_{0,0}q_{n,m}}{(n^2+m^2)^{5/2}}(x_{0,0}(x_{n,m}(n^2-2m^2) \\ &\quad +3nmy_{n,m}) + y_{0,0}(y_{n,m}(m^2-2n^2) \\ &\quad +3nmx_{n,m})). \end{aligned} \quad (4)$$

Here, R_0 is the root-mean-square radius of the vortex core trajectory and $\varepsilon = \mu_0 M^2/\left(R_0^2 d^3\right)$. Note that the combinations of the signs of chirality q and polarity p determines the direction of the effective magnetic moment of a disk at the core shift and direction of rotation of the core around the square center (clockwise or counterclockwise) [37,50].

The expression for the Zeeman energy of one element with indices $\{n, m\}$ is

$$U_H = -\mathbf{M}_{n,m}(\mathbf{H} + \mathbf{h}_0(t)). \quad (5)$$

Here, $\mathbf{H} = H_z\mathbf{k} = hH_S\mathbf{k}$ is the dc external magnetic field perpendicular to the film plane. The quantity $\mathbf{h}_0(t) = h_0(t)\mathbf{j}$ is the small variable component of the external field parallel to the Y axis (the unit vector is $\mathbf{j}$). Then, according to Figure 4, we obtain the energy U_H

$$U_H = U_0 - \mathbf{M}_{n,m}\mathbf{h}_0(t) = U_0 - \frac{q_{n,m}Mh_0(t)}{R_0}x_{n,m}. \quad (6)$$

The quantity $U_0 = -\mathbf{M}_{n,m}\mathbf{H}_z = -M_zH_z$ in the steady-state core motion regime is stable in time and independent of the core radius vector $\mathbf{r}$.

According to (4) and (6), for equation (1) we obtain the system of equations (for the sake of briefness, indices $\{0,0\}$ are omitted)

$$\begin{aligned} -Gv_y - Dv_x - \kappa x + F_{dip_x} + f_x = 0, \\ Gv_x - Dv_y - \kappa y + F_{dip_y} = 0. \end{aligned} \quad (7)$$

Here, we introduced the designations

$$\begin{aligned} F_{\mathrm{dip}_x} &= -\frac{\partial U_{\mathrm{dip}}}{\partial x} = -\varepsilon\sum_{(n+m)\neq 0}qq_{n,m}\left(\frac{n^2-2m^2}{(n^2+m^2)^{5/2}}x_{n,m}\right. \\ &\quad \left.+\frac{3nm}{(n^2+m^2)^{5/2}}y_{n,m}\right), \\ F_{\mathrm{dip}_y} &= -\frac{\partial U_{\mathrm{dip}}}{\partial y} = -\varepsilon\sum_{(n+m)\neq 0}qq_{n,m}\left(\frac{m^2-2n^2}{(n^2+m^2)^{5/2}}y_{n,m}\right. \\ &\quad \left.+\frac{3nm}{(n^2+m^2)^{5/2}}x_{n,m}\right), \\ f_x &= -\frac{\partial U_H}{\partial x} = \frac{qM}{R_0}h_0(t). \end{aligned} \quad (8)$$

For further calculations, we assume the variable component of the external field to change in accordance with the harmonic law $h_0(t) = \eta\cos(-\omega t + \varphi_0)$. We seek for the solutions of system of equation (7) in the form $x_{n,m} = x_{0_{n,m}}\cos(-\omega_{n,m}t + \mathbf{K}\mathbf{r}_{n,m})$, $y_{n,m} = y_{0_{n,m}}\sin(-\omega_{n,m}t + \mathbf{K}\mathbf{r}_{n,m})$. Here, $\mathbf{K}$ is the wave vector. Note that the frequencies $\omega_{n,m}$ of different elements in the steady-state mode have the same value and their sign is determined by the parameter π_T.

Now, let us consider a particular case of distribution of the parameters p and q. We assume the array to only contain elements of two sorts with the parameters $\{p_1, q_1\}$ and $\{p_2, q_2\}$ (the model of an island from elements with

a certain π_T distribution). They are positioned symmetrically relative to the X and Y axes. The example of such a distribution is the chessboard structure, where any pair of nearest elements has the same combination $\{p_1, p_2, q_1, q_2\}$. Assuming the distribution of parameters of the elements to be symmetric, we significantly simplify the calculation of sums in equations (8).

Substituting the trial solutions into equations (7) for the elements of both sorts, we arrive at

$$\begin{aligned}
G_1\omega y_{0_1} + (iD\omega+\kappa)x_{0_1} &= \frac{q_1 M\eta}{R_0}e^{i\varphi_0} - \varepsilon x_{0_1}S_1^{(1)} \\
&\quad -\varepsilon x_{0_2} q_1 q_2 S_1^{(2)}, \\
G_1\omega x_{0_1} + (iD\omega+\kappa)y_{0_1} &= -\varepsilon y_{0_1}S_2^{(1)} - \varepsilon y_{0_2} p_1 p_2 S_2^{(2)}, \\
G_2\omega y_{0_2} + (iD\omega+\kappa)x_{0_2} &= \frac{q_2 M\eta}{R_0}e^{i\varphi_0} - \varepsilon x_{0_2}S_1^{(1)} \\
&\quad -\varepsilon x_{0_1} q_1 q_2 S_1^{(2)}, \\
G_2\omega x_{0_2} + (iD\omega+\kappa)y_{0_2} &= -\varepsilon y_{0_2}S_2^{(1)} - \varepsilon y_{0_1} p_1 p_2 S_2^{(2)}. \quad (9)
\end{aligned}$$

Here, we introduced the following designations for the sums:

$$\begin{aligned}
S_1^{(1)} &= \sum_{\substack{(n+m)\neq 0 \\ \text{by first type}}} \frac{n^2-2m^2}{(n^2+m^2)^{5/2}} \\
&\quad \times \cos(K_x nd)\cos(K_y md), \\
S_1^{(2)} &= \sum_{\substack{(n+m)\neq 0 \\ \text{by second type}}} \frac{n^2-2m^2}{(n^2+m^2)^{5/2}} \\
&\quad \times \cos(K_x nd)\cos(K_y md), \\
S_2^{(1)} &= \sum_{\substack{(n+m)\neq 0 \\ \text{by first type}}} \frac{m^2-2n^2}{(n^2+m^2)^{5/2}} \\
&\quad \times \cos(K_x nd)\cos(K_y md), \\
S_2^{(2)} &= \sum_{\substack{(n+m)\neq 0 \\ \text{by second type}}} \frac{m^2-2n^2}{(n^2+m^2)^{5/2}} \\
&\quad \times \cos(K_x nd)\cos(K_y md). \quad (10)
\end{aligned}$$

The summation should be made according to the sort of an element. For example, the summation $S_1^{(1)}$ should be made over squares with the parameters p_1 and q_1.

Using system of equation (9), we determine the complex amplitudes $\{x_{0_1}, y_{0_1}, x_{0_2}, y_{0_2}\}$. For example, the trajectory of the magnetic vortex core motion for the element of the first sort is similar to an ellipse with the semi-axes $R_{0_x} = |x_{0_1}|$, $R_{0_y} = |y_{0_1}|$, where

$$\begin{aligned}
x_{0_1} &= \frac{q_1 M\eta}{R_0}e^{i\varphi_0}\left[\left(\left(iD\omega+\kappa+\varepsilon S_2^{(1)}\right)^2 - \varepsilon^2 S_2^{(2)2}\right)\right. \\
&\quad \times \left(iD\omega+\kappa+\varepsilon S_1^{(1)} - \varepsilon S_1^{(2)}\right) \\
&\quad \left. + G_2^2\omega^2\left(iD\omega+\kappa+\varepsilon S_2^{(1)}\right) + G_1 G_2\omega^2\varepsilon S_2^{(2)}\right]/Z,
\end{aligned}$$

$$\begin{aligned}
y_{0_1} &= \frac{p_1 M\eta\omega}{R_0}e^{i\varphi_0}\left[\left(G_2\varepsilon S_2^{(2)} - G_1\left(iD\omega+\kappa+\varepsilon S_2^{(1)}\right)\right)\right. \\
&\quad \left. \times \left(iD\omega+\kappa+\varepsilon S_1^{(1)} - \varepsilon S_1^{(2)}\right) + G_1 G_2^2\omega^2\right]/Z. \quad (11)
\end{aligned}$$

Denominator Z is of the form:

$$\begin{aligned}
Z &= -G_1^2 G_2^2\omega^4 + \left(iD\omega+\kappa+\varepsilon S_1^{(1)}\right)\left(iD\omega+\kappa+\varepsilon S_2^{(1)}\right) \\
&\quad \times \left(G_1^2+G_2^2\right)\omega^2 + 2G_1 G_2\omega^2\varepsilon^2 S_1^{(2)} S_2^{(2)} \\
&\quad - \left(\left(iD\omega+\kappa+\varepsilon S_1^{(1)}\right)^2 - \varepsilon^2 S_1^{(2)2}\right) \\
&\quad \times \left(\left(iD\omega+\kappa+\varepsilon S_2^{(1)}\right)^2 \varepsilon^2 S_2^{(2)2}\right). \quad (12)
\end{aligned}$$

Similarly, we obtained the expressions for x_{0_2} and y_{0_2}.

It is interesting to discuss some particular cases. In the absence of interactions between elements, we have $\varepsilon \to 0$. Then, according to (11), we have for the array of elements of the first sort

$$\begin{aligned}
R_{0_x} &= \frac{q_1 M\eta}{R_0\kappa}\sqrt{\frac{\omega_0^4 + \Gamma^2\omega^2}{(\omega^2-\omega_0^2)^2 + 4\Gamma^2\omega^2}}, \\
R_{0_y} &= \frac{p_1 M\eta}{R_0\kappa^2}\frac{G_1\omega_0^2\omega}{\sqrt{(\omega^2-\omega_0^2)^2 + 4\Gamma^2\omega^2}}. \quad (13)
\end{aligned}$$

Here, we use the designations from [4]: $\omega_0^2 = \kappa^2/(G_1^2 + D^2)$ and $\Gamma = D\kappa/(G_1^2+D^2)$. In the ideal case, the core trajectory at $\Gamma \to 0$ tends to the circumference $R_{0_x} \approx R_{0_y}$; in the other cases, the trajectory is almost elliptical.

In the general case, the functions $R_{0_x}(\omega)$ and $R_{0_y}(\omega)$ have the resonant form. The resonant frequencies are determined not only by the characteristics of separate squares (G, κ and Γ), but also by the rigidity of the magnetostatic coupling, which depends on the ε value and sums (10). Elimination of the degeneracy of frequencies with different combinations of the polarities and chiralities is explained by the presence of the terms with the product $G_1 G_2$ in the uneven degrees in equations (11) and (12). In addition, the absolute values of parameters G, κ, and Γ depend on the perpendicular component of the magnetic field; consequently, its variation leads to the change in ω_0 and shift of the resonance peak.

Thus, the occurrence of several peaks in the experimental absorption curves $P(h)$ with a decrease in the distance between array elements can be attributed to the increasing interplay of elements. In the model of noninteracting magnets, the resonance behavior of magnetization will only be demonstrated by elements with the same (favorable) core polarity. Therefore, we would fix the only resonant frequency. At the generator frequency in the range of $\omega > \omega_0$, the favorable polarity direction is parallel to the magnetic field and, at $\omega < \omega_0$, is antiparallel to it [10]. The chirality sign only affects the core rotation direction. When there is the interaction between the magnetic subsystems of elements, the collective motion of cores in the normal modes can be implemented. In zero external field, ignoring the

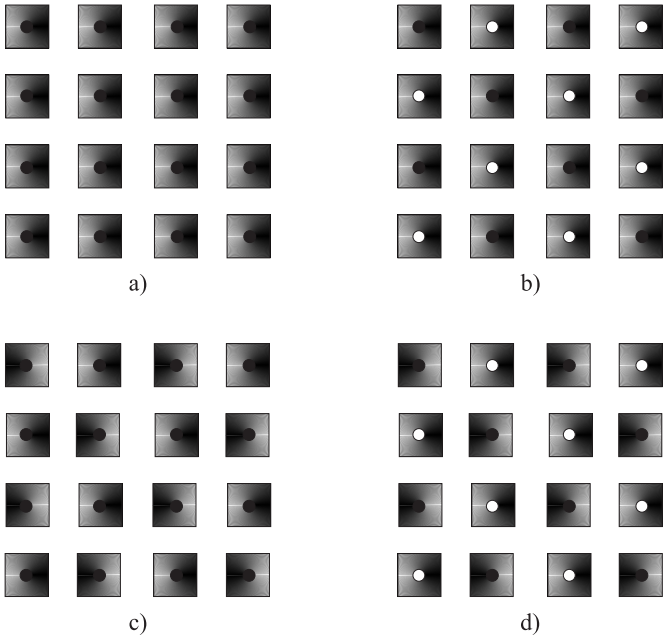

Fig. 5. Examples of possible combinations of polarities and chiralities of elements $\{p_1, p_2, q_1, q_2\}$ in the chessboard arrays: (a) $\{1,1,1,1\}$, (b) $\{1,-1,1,1\}$, (c) $\{1,1,1,-1\}$, and (d) $\{1,-1,1,-1\}$. The chiralities of elements are conventionally denoted by different filling directions. The core polarity directions are shown with black and white filling of the central region of squares.

dissipation ($D \ll G$), we can easily determine the resonant frequencies from the condition $|Z| = 0$. As a result, we obtain

$$\omega^2 = \frac{1}{G^2}\left(\kappa + \varepsilon S_1^{(1)} \pm \pi_T \varepsilon S_1^{(2)}\right)\left(\kappa + \varepsilon S_2^{(1)} \pm \pi_T \varepsilon S_2^{(2)}\right). \tag{14}$$

This is consistent with the calculations from [24,25].

The chessboard distribution of the topological charge of elements is most frequently implemented during film fabrication [51]. Figure 5 shows four possible combinations of p and q, which make the main contribution to the absorption curve. Note that each of the four states shown in the figure ensures its own vibration frequency, but these frequencies are degenerate in the long-wavelength limit.

Indeed, the four different frequencies can be obtained using the following combinations: $\{p_1, p_2, q_1, q_2\}$:

$$\begin{aligned}
&\omega_1 : \{1,1,1,1\}, \{1,1,-1,-1\},\\
&\omega_2 : \{1,1,1,-1\}, \{1,1,-1,1\},\\
&\omega_3 : \{1,-1,1,1\}, \{1,-1,-1,-1\}, \{-1,1,1,1\},\\
&\qquad \{-1,1,-1,-1\},\\
&\omega_4 : \{1,-1,1,-1\},\\
&\qquad \{1,-1,-1,1\}\{-1,1,1,-1\}\{-1,1,-1,1\}.
\end{aligned}$$

For the absorbed power of a pair of squares with a certain combination $\{p_1, p_2, q_1, q_2\}$, we can write

$$P(h)_{\{p_1,p_2,q_1,q_2\}} = D\omega^2\left(|x_{0_1}|^2 + |y_{0_1}|^2 + |x_{0_2}|^2 + |y_{0_2}|^2\right). \tag{15}$$

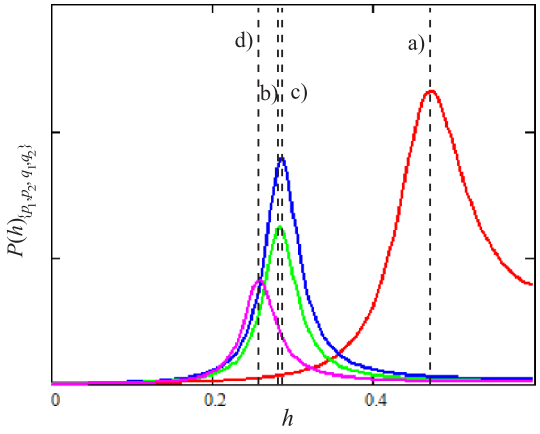

Fig. 6. Resonance curves for the modes that make the main contribution to the absorbed power curve. In the calculation, we used the following values of magnetic characteristics: $M_S = 770$ G, $\alpha = 0.01$ is the damping parameter, $\omega = 415$ MHz, $M \approx M_S aL$, and $R_0 \approx L/2$. The designations of the curves correspond to Figure 5.

Curves (15) are presented in Figure 6.

The real array contains islands with different combinations shown in Figure 5, therefore, we can write the estimating expression for the total power

$$P(h) = \sum_{a,b,c,d} \rho_{\{p_1,p_2,q_1,q_2\}} P(h)_{\{p_1,p_2,q_1,q_2\}}. \tag{16}$$

Here, $\rho_{\{p_1,p_2,q_1,q_2\}}$ is the quantitative fraction of pairs of elements with the corresponding combination $\{p_1, p_2, q_1, q_2\}$ and the summation is made over the states shown in Figure 5.

The ρ value is used as a fitting parameter. In the long-wavelength limit ($K_x = K_y = 0$), the $P(h)$ curves obtained using equation (16) with regard to equations (11) and analogous expressions for x_{0_2}, y_{0_2} are shown in Figure 7. In the estimation of the quasielastic force coefficient, we used the expression $\kappa = \xi\mu_0 M_S^2 L^2(1-h^2)/a$, where a is the square side length and ξ is the dimensionless fitting parameter (about unity) [11]. The ξ value was chosen such as to the curve (16) fitted best the experimental curve in Figure 7a.

4 Conclusions

The occurrence of several resonance peaks with decreasing distance between elements suggests the magnetostatic nature of the FMR frequency splitting. At the large distance between elements of the array, the frequencies of normal vibrational modes of magnetization weakly differ from the resonant frequency of the core motion in an individual element due to the weakness of interaction between elements. In this case, the absorption curves are superimposed and yield the only visual maximum (frequency degeneracy), which can be seen in Figures 2a and 7a. As the distance between elements in the array decreases, the coupling between magnetic moments of elements becomes

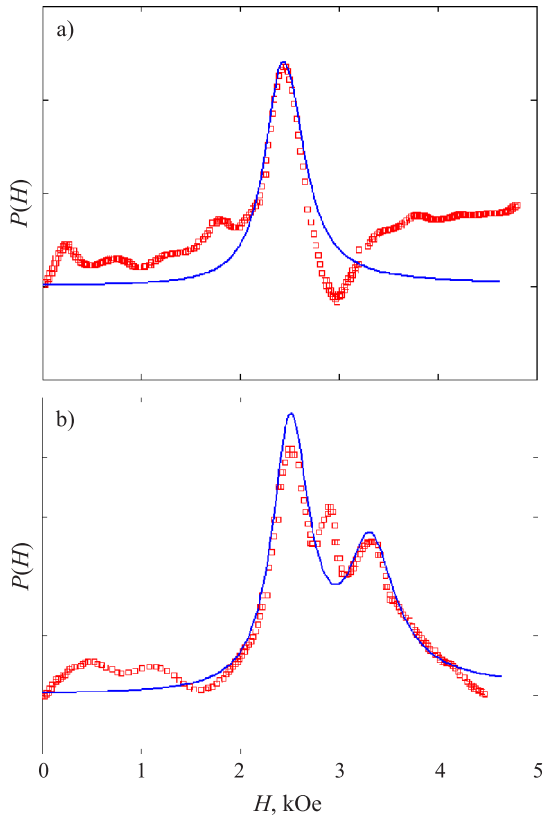

Fig. 7. Integral absorption curves obtained from the experimental data in comparison with calculated absorption power (16). The results of integration of the experimental curves (Fig. 2) are shown by square dots and the theoretical curve, by the solid line.

significant. In this case, the differences between the frequencies of normal modes are so large that the separate peaks arise in the absorption curves.

The quantitative discrepancy between the calculation using equation (16) and experimental curve (Fig. 7) can be attributed to the several factors, specifically, (i) disregarding the magnetostatic interaction between the core magnetic moments, (ii) noncylindrical symmetry of the potential, where the core is located as a quasiparticle (such a shape of the element ensures the in-plane anisotropy with the easy-axis direction changing with the distance between elements [52]), (iii) the error caused by the rigid vortex core model used, and (iv) the importance of using the quadrupole term in calculating the magnetostatic interaction energy for a square-shaped element [24,53]. Moreover, as was shown in [24], at the significant core vibration amplitudes, the strict calculation of the interaction energy should take into account not only the dipole-dipole, but also dipole-octupole, octupole-octupole, etc. approximations. It is worth noting that the account for the above-mentioned factors will make quantitative corrections without changing the general picture. In a real array, there are areas not only with chessboard distribution p and q. The areas with other symmetrical and nonsymmetric distributions are possible [25]. Such areas have sets of frequencies that do not coincide with (14) and they may be responsible for the existence of the third peak in Figure 7. The complex account for these factors will be discussed in the next studies.

To sum up, note that the strong interplay of elements can prevent finding a reliable method for controlling the magnetization state (polarity and chirality) in arrays of closely packed elements, which is of great importance for spintronic applications, especially at the external field frequencies similar to the eigenfrequencies. At the same time, this interplay opens the possibility of simultaneous governing the state of a whole set of elements united by one vibrational mode. Anyway, when designing devices based on large arrays of nanosized elements, the interplay of their magnetic moments must not be ignored.

This study was supported by the Russian Foundation for basic research, project no. 16-32-00103 and, in part, project no. 18-02-00161.

Author contribution statement

The contributions of all authors are equal.

References

1. W. Scholz, K.Yu. Guslienko, V. Novosad, D. Suess, T. Schrefl, JMMM **266**, 155 (2003)
2. A. Thiele, Phys. Rev. Lett. **30**, 230 (1973)
3. B. Ivanov, G. Avanesyan, A. Khvalkovskiy, N. Kulagin, C. Zaspel, K. Zvezdin, JETP Lett. **91**, 178 (2010)
4. J. Kim, S.-B. Choe, J. Magn. **12**, 113 (2007)
5. A. Puzic, B. Van Waeyenberge, K. Chou, P. Fischer, H. Stoll, G. Schutz, T. Tyliszczak, K. Rott, H. Bruckl, G. Reiss, I. Neudecker, Th. Haug, M. Buess, C. Back, J. Appl. Phys. **97**, 10E704 (2005)
6. B. Pigeau, G. De Loubens, O. Klein, A. Riegler, F. Lochner, G. Schmidt, L. Molenkamp, V. Tiberkevich, A. Slavin, Appl. Phys. Lett. **96**, 132506 (2010)
7. K. Guslienko, V. Novosad, Y. Otani, H. Shima, K. Fukamichi, Phys. Rev. B **65**, 024414 (2001)
8. J. Park, P. Eames, D. Engebretson, J. Berezovsky, P. Crowell, Phys. Rev. B **67**, 020403(R) (2003)
9. S. Vdovichev, B. Gribkov, S. Gusev, V. Mironov, D. Nikitushkin, A. Fraerman, V. Shevtsov, Phys. Solid State **48**, 1902 (2006)
10. G. Loubens, A. Riegler, B. Pigeau, F. Lochner, F. Boust, K. Guslienko, H. Hurdequint, L. Molekamp, G. Schmidt, A. Slavin, S. Tiberkevich, N. Vukadinovic, O. Klein, Phys. Rev. Lett. **102**, 177602 (2009)
11. P. Kim, V. Orlov, R. Rudenko, V. Prokopenko, I. Orlova, A. Kobyakov, J. Magn. Magn. Mater. **440**, 171 (2017)
12. V. Prokopenko, P. Kim, V. Orlov, B. Vasiliev, D. Vovk, S. Zatsepilin, R. Rudenko, J. Sib. Fed. Univ. Math. Phys. **6**, 262 (2013)
13. S. Erokhin, D. Berkov, Phys. Rev. B **89**, 144421 (2014)
14. S. Sugimoto, Y. Fukuma, S. Kasai, T. Kimura, A. Barman, Y. Otani Phys. Rev. Lett. **106**, 197203 (2011)
15. B. Van Waeyenberge, A. Puzic, H. Stoll, K. Chou, K. Tyliszczak, R. Hertel, M. Fahnle, H. Bruckl, K. Rott, G. Reiss, I. Neudecer, D. Weiss, C. Back, G. Schutz, Nat. Lett. **444**, 206 (2006)

16. A. Vogel, T. Kamionka, M. Martens, A. Drews, K. Chou, T. Tyliszczak, H. Stoll, B. Van Waeyenberge, G. Meier, Phys. Rev. Lett. **106**, 137201 (2011)
17. S. Choe, Y. Acremann, A. Scholl, A. Bauer, A. Doran, J. Stohr, H. Padmore, Science **304**, 420 (2004)
18. F. Peng, D. Hui, Ann. Phys. **523**, 417 (2011)
19. M. Konoto, T. Yamada, K. Koike, H. Akoh, T. Arima, Y. Tokura, J. Appl. Phys. **103**, 023904 (2008)
20. Yu. Gorobets, Yu. Dzhezherya, A. Kravets, Phys. Solid State **42**, 126 (2000)
21. J. Dou, S. Hernandez, Ch. Yu , M. Pechan, L. Folks, J. Katine, M. Carey, J. Appl. Phys. **107**, 09B514 (2010)
22. A. Galkin, B. Ivanov, C. Zaspel, Phys. Rev. B **74**, 144419 (2006)
23. A. Galkin, B. Ivanov, J. Exp. Theor. Phys. **109**, 74 (2009)
24. O.V. Sukhostavets, J. Gonzalez, K.Y. Guslienko, Phys. Rev. B **87**, 094402 (2013)
25. R. Verba, G. Melkov, V. Tiberkevich, A. Slavin, Phys. Rev. B **85**, 014427 (2012)
26. P.V. Bondarenko, A.Yu. Galkin, B.A. Ivanov, C.E. Zaspel, Phys. Rev. B **81**, 224415 (2010)
27. J. Shibata, Y. Otani, Phys. Rev. B **70**, 012404 (2004)
28. H. Jung, Y. Yu, K. Lee, M. Im, P. Fischer, L. Bocklage, A. Vogel, M. Bolte, G. Meier, S. Kim, Appl. Phys. Lett. **97**, 222502 (2010)
29. K. Lee, H. Jung, D. Han, S. Kim, J. Appl. Phys. **110**, 113903 (2011)
30. D. Han, A. Vogel, H. Jung, K. Lee, M. Weigand, H. Stoll, G. Schutz, P. Fischer, G. Meier, S. Kim, Sci. Rep. **3**, 2262 (2013)
31. P. Kim, V. Orlov, R. Rudenko, V. Prokopenko, I. Orlova, S. Zamai, JETP Lett. **101**, 562 (2015)
32. O. Klein, G. De Loubens, V. Naletov, F. Boust, T. Guillet, H. Hurdequint, A. Leksikov, A. Slavin, V. Tiberkevich, N. Vukadinovic, Phys. Rev. B **78**, 144410 (2008)
33. K. Lee, S. Kim, Appl. Phys. Lett. **91**, 132511 (2007)
34. V. Kravchuk, Yu. Gaididei, D. Sheka, Phys. Rev. B **80**, 100405(R) (2009)
35. K. Lee, K. Guslienko, J. Lee, S. Kim, Phys. Rev. B **76**, 174410 (2007)
36. B. Ivanov, G. Wysin, Phys. Rev. B **65**, 134434 (2002)
37. K. Guslienko, B. Ivanov, V. Novosad, Y. Otani, H. Shima, K. Fukamichi, J. Appl. Phys. **91**, 8037 (2002)
38. B. Ivanov, E. Galkina, A. Galkin, Low Temp. Phys. **36**, 747 (2010)
39. A. Zvezdin, K. Zvezdin, Low Temp. Phys. **36**, 826 (2010)
40. R. Elias, A. Verga, Phys. Rev. B **89**, 134405 (2014)
41. E. Galkina, B. Ivanov, V. Stephanovich, J. Magn. Magn. Mater. **118**, 373 (1993)
42. P. Kim, V. Orlov, V. Prokopenko, S. Zamai, V. Prints, R. Rudenko, T. Rudenko, Phys. Solid State **57**, 30 (2015)
43. A. Belanovsky, N. Locatelli, P. Skirdkov, F. Abreu Araujo, J. Grollier, K. Zvezdin, V. Cros, A. Zvezdin, Phys. Rev. B **85**, 100409(R) (2012)
44. B. Ivanov, C. Zaspel, Phys. Rev. Lett. **99**, 247208 (2007)
45. S. Cherepov, B. Koop, V. Korenivski, D. Worledge, A. Galkin, R. Khymyn, B. Ivanov, Phys. Rev. Lett. **109**, 097204 (2012)
46. K. Guslienko, X. Han, D. Keavney, R. Divan, S. Bader, Phys. Rev. Lett. **96**, 067205 (2006)
47. M. Wolf, U. Robler, R. Schafer, J. Magn. Magn. Mater. **314**, 105 (2007)
48. A. Vogel, A. Drews, T. Kamionka, M. Bolte, G. Meier, Phys. Rev. Lett. **105**, 037201 (2010)
49. J. Shibata, K. Shigeto, Y. Otani, Phys. Rev. B **67**, 224404 (2003)
50. À. Mertens, A. Bishop, arXiv:cond-mat/9903037v1 (1999)
51. A. Galkin, B. Ivanov, A. Merkulov, J. Exp. Theor. Phys. **101**, 1106 (2005)
52. L. Sun, X. Zou, W. Zhang, G. Li, Ya. Zhai, J. Wu, Y. Xu, H. Zhai, Phys. Status Solidi C **9**, 66 (2012)
53. C. Phatak, R. Pokharel, M. Beleggia, M. De Graef, JMMM **323**, 2912 (2011)